Utilizing Multipath Effects for Mobile Charging

Jing Gao, Die Wu, *Member, IEEE*, Linglin Zhang, Jingwen Li, Jin Yang, Jian Peng, *Member, IEEE*, and Tang Liu, *Member, IEEE*

***Abstract*—Recently, Wireless Rechargeable Sensor Networks (WRSNs) have emerged as a promising solution to address the energy limitations of wireless sensor networks. In practical applications of WRSNs, environmental objects are ubiquitous, reflecting radio waves and causing them to reach sensors via multiple paths. These multipath effects significantly impact the power intensity received by sensors. In this paper, we study a fundamental issue of charGing schEduling with mulTipath effectS (GETS), that is, how to schedule a mobile charger by comprehensively considering the multipath effects to maximize the overall charging utility. To this end, we first establish a charging model with environmental objects to investigate the impact of multipath effects on power distribution. Then, we propose a charging scheduling scheme that not only selects a series of sojourn locations for the MC (Mobile Charger) to maximize the total power received by nearby sensors but also construct a charging path that avoids environmental objects. We conduct extensive simulations as well as indoor and outdoor field experiments to evaluate the performance of our scheme. The results demonstrate that, on average, our scheme outperforms baseline algorithms by 48.87% .**

***Index Terms*—Wireless power transfer, multipath effects, charging scheduling, wireless rechargeable sensor networks.**

I. Introduction

RECENTLY, Wireless Power Transfer (WPT) [1] has emerged as a transformative technology for enabling wireless power supply. The Wireless Power Consortium (WPC), an organization committed to standardizing WPT, has garnered active participation from leading companies such as Microsoft, Qualcomm, Samsung, and Google [2]. As reported in [3], the global wireless charging market, valued at 21.44 billion in 2023, is projected to grow significantly, reaching 71.47 billion by 2030.

Among the diverse applications of WPT, Wireless Rechargeable Sensor Networks (WRSNs) have gained prominence in various domains, including smart homes, industrial automation, healthcare, and other fields [4], [5], [6], [7], [8], [9], [10]. In a typical WRSN, a Mobile Charger (MC) equipped with antennas and batteries is scheduled to traverse a pre-determined charging path comprising a series of sojourn locations. At each sojourn location, the MC wirelessly transmits radio waves to charge surrounding sensors, thereby extending their operational lifetimes [11], [12], [13], [14].

Much effort has been devoted to optimizing the charging scheduling of the MC to achieve efficient wireless charging. Traditional scheduling methods typically focus on selecting appropriate sojourn locations [15], [16], [17], [18] or shortening charging path [19], [20], [21], [22], [23] to ensure that sensors receive sufficient power in an ideal and open environment. However, in practical applications, environmental objects with arbitrary shapes, materials, and sizes are ubiquitous. For instance, in outdoor scenarios, environmental objects such as trees, walls, and electric poles reflect the radio waves from the MC, leading to significant multipath effects. As a result, the actual power received by the sensors can differ substantially from the theoretical value that disregards environmental factors. Similarly, in indoor charging scenarios, radio waves emitted by the MC are reflected by furniture, walls, and electrical appliances, also bringing multipath effects and altering the power received by the sensors. Therefore, we can see that traditional charging scheduling methods ignore environmental objects, making it difficult for them to adapt to real-world environments.

Recently, a few pioneering researchers have begun to focus on the impacts of environmental objects on charging efficiency in practice. For example, Wang et al. [24] and You et al. [25] revealed that environmental objects can block the propagation of radio waves, while Lin et al. [26] observed the diffraction phenomenon caused by such objects. Additionally, Yang et al. [27] explored the utilization of wave reflection for non-line-of-sight charging. However, these studies share a common problem: they overlook the multipath effects caused by wave reflections from environmental objects. The waves transmitted via the reflected path interfere with the direct path waves, leading to a discrepancy between the theoretical and practical power received by the sensors.

Fig. 1 illustrates the multipath effects caused by environmental objects in a typical indoor charging scenario. It can be seen that two sensors are located near two walls, and an MC is situated between them for recharging. The radio waves emitted by the MC travel along direct paths (*i.e.*, blue solid lines) and then reach the sensors. Moreover, reflected waves from two walls also propagate along the reflected paths (*i.e.*,

Received 22 January 2025; revised 13 March 2025; accepted 26 March 2025. Date of publication 3 April 2025; date of current version 6 August 2025. This work was supported in part by the National Natural Science Foundation of China under Grant 62072320, Grant 62002250, and Grant 62306201, and in part by the Natural Science Foundation of Sichuan Province under Grant 2022NSFSC0569, Grant 2025ZNSFSC1466, and Grant 2025ZNSFSC0501. Recommended for acceptance by H. Wu. *(Corresponding author: Tang Liu.)*

Jing Gao, Die Wu, Linglin Zhang, Jingwen Li, and Tang Liu are with the College of Computer Science, Sichuan Normal University, Chengdu 610101, China, and also with the Visual Computing and Virtual Reality Key Laboratory of Sichuan Province, Sichuan Normal University, Chengdu 610068, China (e-mail: jinggao@stu.sicnu.edu.cn; wd@sicnu.edu.cn; linglinzhang@stu.sicnu.edu.cn; lijingwen@sicnu.edu.cn; liutang@sicnu.edu.cn).

Jin Yang is with the School of Cyber Science and Engineering, Sichuan University, Chengdu 610065, China (e-mail: yangjin66@scu.edu.cn).

Jian Peng is with the College of Computer Science, Sichuan University, Chengdu 610065, China (e-mail: jianpeng@scu.edu.cn).

Digital Object Identifier 10.1109/TMC.2025.3557899

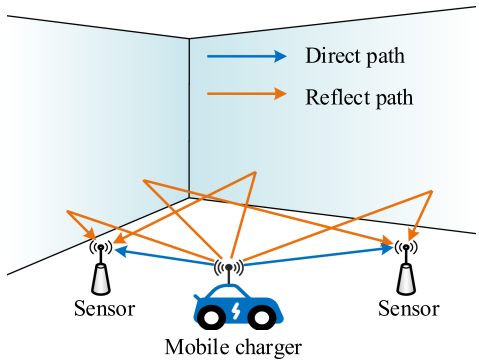

Fig. 1. A typical indoor charging scenario.

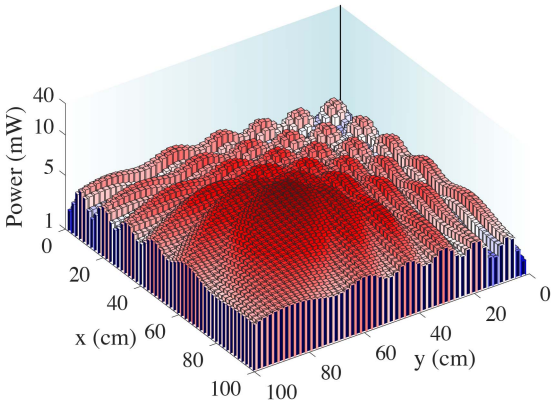

Fig. 2. A field experiment on power distribution with two perpendicular walls. The vertical distance between the charger and each wall was 60 cm. The 1 m × 1 m experimental area was divided into 2 cm × 2 cm grids and the sensor was sequentially placed at the center of each grid to record the received power. Both the charger and the sensor are produced by Powercast [28].

orange solid lines) to the sensors. Since interference occurs as these waves from different paths converge, the power received by the sensors differs significantly from the value without environmental objects. We conducted a field experiment to explore the power distribution near two walls, as shown in Fig. 2. It can be observed that the reflections from the walls create a complex power distribution around the charger, resulting in alternating high-power and low-power regions.

In this paper, we explore the impact of multipath effects caused by ubiquitous environmental objects on the power received by sensors in practical scenarios. Specifically, we aim to utilize the multipath effects to enhance the power received by sensors. Thus, we state the problem of charGing schEduling with mulTipath effectS (GETS) as follows: given a set of sensors and a number of environmental objects, how to schedule the MC to maximize the overall charging utility of the entire network.

Generally, there are three major challenges in our problem.

The first challenge is the power distribution caused by the multipath effects is very complex. The complexity results from *(i)* the charging power is nonlinear with distance; *(ii)* the interference caused by multipath propagation is also nonlinear. Additionally, the number, size, material, and position of objects in the environment are arbitrary, which further increases the complexity of power distribution.

The second challenge lies in that the network space is continuous, resulting in infinite feasible sojourn locations for MC. This also leads to an infinite number of positional relationships between the MC and environmental objects, which determine the nonlinear power distribution.

The third challenge is how to design an effective scheduling algorithm for MC. As the battery capacity of MC is limited, scheduling the charging path for MC is similar to solving an NP-hard Traveling Salesman Problem (TSP). Besides that, the charging path should avoid all environmental objects in WRSNs.

To address the first challenge, we develop a practical charging model that integrates multipath effects resulting from environmental objects, enabling us to analyze patterns of high power distribution influenced by these effects.

To tackle the second challenge, the underlying mechanism of our method is network dividing and area discretization techniques. Specifically, network dividing involves identifying potential sojourn areas for the MC based on the spatial distribution of sensors and further subdividing these areas into multiple subregions by considering the spatial relationships between sensors and environmental objects. Discretization refers to approximating the nonlinear charging power distribution with piecewise constant segments, effectively dividing the subregions into a finite number of fine-grained regions, thereby reducing the infinite solution space to a finite solution space.

As for the third challenge, we transform the GETS problem into a submodular function maximization problem with energy constraints. Then, we propose a greedy-based charging path planning algorithm to select a series of sojourn locations, constructing a shortest charging path that can avoid environmental objects.

The main contributions of this work are summarized below.

- To the best of our knowledge, we are the first to leverage the multipath effects caused by environmental objects to enhance charging efficiency. To investigate the impact of multipath effects on power distribution, we establish a practical charging model that incorporates these objects.
- To solve the GETS problem, we first identify candidate sojourn locations that could maximize the total power received by nearby sensors, then we construct a shortest charging path that avoids obstacles, achieving an approximation ratio of $\frac{1}{2}(1-e^{-1})$ with a slightly relaxed budget.
- To evaluate our scheme, extensive simulations as well as indoor and outdoor field experiments are conducted. The results show that, on average, our scheme outperforms the baseline by 48.87% .

The remainder of the paper is organized as follows. Section II introduces the network model, charging model with environmental objects, and problem formulation. Section III explains how multipath effects are leveraged to maximize the overall charging utility. Sections IV and V evaluate the performance of our proposed scheme through simulations and field experiments. Section VI reviews the related work. Finally, we conclude our work in Section VII.

TABLE I
MAJOR NOTATIONS

Notation	Meaning
C	Mobile charger, or its location
s_i	Rechargeable sensor i, or its location
o^g	Fixed environmental object g, or its location
l_j	Sojourn location j
S	Sensor set of all the sensors in the network
D	The longest charging distance of MC
O	Object set of all the objects in the network
S_{l_j}	Sensor set include the sensors covered by MC at l_j
d_{C,s_j}	Distance between MC and sensor s_i
d_{C,o^g}	Distance between MC and object o^g
d_{o^g,s_j}	Distance between object o^g and sensor s_i
$\hat{d}$	attenuation factor in the propagation of the wave
λ	Wavelength of the radio waves
A	Amplitude of the radio waves
Γ^g	attenuation of the reflected wave on object o^g
P_{s_i}	Power received by s_i
P_{th}	Threshold of received power for sensor
P_0	Transmission power of MC
B	Battery capacity of MC
$\mathcal{C}$	Total cost of MC in one charging cycle
L	Candidate sojourn location set
$\mathcal{H}$	Charging path or sojourn location set

II. PRELIMINARIES

In this section, we present the network model, charging model with environmental objects, cost model, charging utility model, and problem formulation. We list the major notations in this paper in Table I.

A. Network Model

We consider a 2D plane network Ω, consisting of a Base Station (BS), a Mobile Charger (MC) with a battery capacity denoted by B, and N stationary sensors denoted by the set S. Each sensor $s_i \in S$ is powered by a battery with an energy capacity b. To simplify the model, we use s_i and C to represent the location of sensor s_i and MC, respectively.

During each charging cycle, the MC departs from BS with full energy, follows a pre-designed charging path, and visits a series of sojourn locations to charge the nearby sensors. For any sojourn location l_j, the sensors located within the charging range of l_j are denoted by the set S_{l_j}. Before the MC's energy is depleted, it returns to the BS to get fully recharged for the next charging cycle.

There are also M fixed environmental objects $O = \{o^1, o^2, \ldots, o^M\}$ distributed in the network. Let Γ^g denote the reflection coefficient of o^g, which represents the ratio between the amplitudes of the reflected wave as it leaves the environmental object and the incident wave as it reaches the object, thereby quantifying the attenuation of signal strength caused by the environmental object during the reflection of the radio wave. o^g can still be used to denote the location of the environmental object o^g. Leveraging existing localization and sensing technology [29], [30], [31], [32], we can acquire the location, shape, and material of each environmental object in advance. We also assume each sojourn location l_j and sensor s_i cannot be located inside these environmental objects.

B. Charging Model With Environmental Objects

To investigate the power distribution in practical charging scenarios, we develop a charging model in this subsection that accounts for the influence of environmental objects on radio waves. Specifically, we first derive the amplitude of the direct wave transmitted from the MC to the sensor and calculate the corresponding power received from this direct wave. Next, we obtain the amplitude of the wave after reflection by environmental objects based on wave reflection properties. Furthermore, we give the amplitude and power of the combined wave received by the sensor when one or more reflected waves from the environmental objects propagate to the sensor. Finally, we quantify the power received by sensors that are partially or fully obstructed by environmental objects.

We begin by expressing the amplitude of the wave emitted from the MC as:

$$A_C(t) = A_0 \cos(\phi_0 + 2\pi f t), \tag{1}$$

where A_0, f and ϕ_0 are denoted as the amplitude, frequency, and initial phase of the wave from MC, respectively.

Since the amplitude attenuates with increasing distance, the amplitude of the wave received by s_i can be expressed as:

$$A_{C,s_i}(t) = \frac{A_0}{\hat{d}_{C,s_i}} \cos\left(\phi_0 + 2\pi f t - \frac{2\pi}{\lambda} d_{C,s_i}\right). \tag{2}$$

In this equation, $\hat{d}_{C,s_i} = \frac{d_{C,s_i}+\beta}{\sqrt{\alpha}}$ is the attenuation factor in the propagation of the wave from MC to sensor s_i, where β is a parameter to adjust the Friis' free space equation for short distance transmission. $\alpha = \frac{G_s G_r \eta}{L_P}(\frac{\lambda}{4\pi})^2$, where G_s and G_r are the antenna gains of MC and sensor, respectively, η is the rectifier efficiency, L_p is the polarization loss, and λ is the wavelength [33]. Assuming that the period of the radio wave is T, the average power at sensor s_i can be written as:

$$\begin{aligned} P_{C,s_i} &= \frac{1}{T}\int_{-\frac{T}{2}}^{\frac{T}{2}} [A_{C,s_i}(t)]^2 \mathrm{d}t \\ &= \frac{1}{T}\int_{-\frac{T}{2}}^{\frac{T}{2}} \left[\frac{A_0}{\hat{d}_{C,s_i}} \cos\left(\phi_0 + 2\pi(ft - \frac{d_{C,s_i}}{\lambda})\right)\right]^2 \mathrm{d}t \\ &= \frac{A_0^2}{2\hat{d}_{C,s_i}^2}. \end{aligned} \tag{3}$$

The waves reflected by environmental objects exhibit two distinct characteristics. First, the amplitude of the reflected wave attenuates due to surface reflections on the environmental objects [34], which possess varying materials. For instance, the oscillation of free electrons induced by radio waves on a metal surface will reflect the incident waves with very low attenuation [34]. Conversely, for the non-conductive materials, the

attenuation will be much greater. To quantify this attenuation, we represent the attenuation of the reflected wave using Γ^g, which signifies the reflection coefficient of the environmental object o^g. Second, the reflected wave undergoes a 180° phase change upon reflection, a phenomenon known as *half-wave loss* [35]. This means that when the incident wave reflects off a denser medium, crests become troughs and vice versa.

Taking these two characteristics into account, we can determine the amplitude of the reflected wave from o^g using the following expression:

$$\begin{aligned} A_{o^g}(t) &= \frac{\Gamma^g A_0}{\hat{d}_{C,o^g}} \cos\left(\phi_0 + 2\pi f t - \frac{2\pi}{\lambda} d_{C,o^g} - \pi\right) \\ &= -\frac{\Gamma^g A_0}{\hat{d}_{C,o^g}} \cos\left(\phi_0 + 2\pi\left(f t - \frac{d_{C,o^g}}{\lambda}\right)\right), \end{aligned} \tag{4}$$

where d_{C,o^g} represents the distance between the MC and the reflection point on o^g, which can be calculated based on the reflection theorem.

Assuming that the combined power received by sensor s_i comprises the direct wave from the MC and a single reflected wave from environmental object o^g, the amplitude of the combined wave can be expressed as:

$$\begin{aligned} &A_{s_i}(t) = A_{C,s_i}(t) + A_{o^g,s_i}(t) \\ &= \frac{A_0}{\hat{d}_{C,s_i}} \cos\left(\phi_0 + 2\pi\left(f t - \frac{d_{C,s_i}}{\lambda}\right)\right) \\ &- \frac{\Gamma^g A_0}{\hat{d}_{C,o^g}\hat{d}_{o^g,s_i}} \cos\left(\phi_0 + 2\pi\left(f t - \frac{(d_{C,o^g} + d_{o^g,s_i})}{\lambda}\right)\right), \end{aligned} \tag{5}$$

where d_{o^g,s_i} is the distance between the reflection point on environmental object o^g and sensor s_i. Since the average power is determined as the ratio of the integral of the amplitude over one period to the duration of the period, the average combined power P_{s_i} received by s_i can be calculated as:

$$\begin{aligned} P_{s_i} &= \frac{1}{T}\int_{-\frac{T}{2}}^{\frac{T}{2}} [A_{s_i}(t)]^2 \mathrm{d}t \\ &= \frac{1}{T}\int_{-\frac{T}{2}}^{\frac{T}{2}} [A_{C,s_i}(t) + A_{o^g,s_i}(t)]^2 \,\mathrm{d}t \\ &= \frac{-\Gamma^g A_0^2}{\hat{d}_{C,s_i}\hat{d}_{C,o^g}\hat{d}_{o^g,s_i}} \cos\frac{2\pi}{\lambda}(d_{C,o^g} + d_{o^g,s_i} - d_{C,s_i}) \\ &+ \frac{A_0^2}{2\hat{d}^2_{C,s_i}} + \frac{\Gamma^{g2} A_0^2}{2\hat{d}^2_{C,o^g}\hat{d}^2_{o^g,s_i}}. \end{aligned} \tag{6}$$

From (6), we observe that the power distribution around environmental object o^g is complex, and certain conditions in the distance relationship between the MC, s_i, and o^g either enhance or weaken the power at s_i. Specifically, when $d_{C,o^g} + d_{o^g,s_i} - d_{C,s_i} = (k + \frac{1}{2})\lambda$, where $k \in \mathbb{N}$, the combined power is enhanced. Conversely, when $d_{C,o^g} + d_{o^g,s_i} - d_{C,s_i} = k\lambda$, where $k \in \mathbb{N}$, the combined power at sensor s_i is weakened.

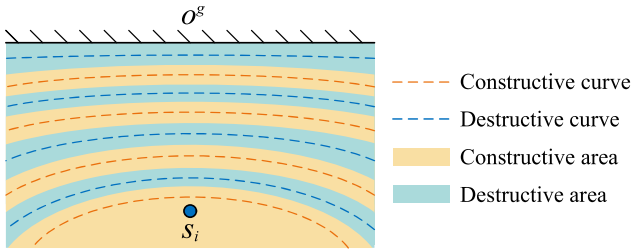

Fig. 3. An illustration of the MC's different location areas.

Since the sensors and environmental objects in the network are fixed, we can only adjust the sojourn location to alter the distance relationship between the MC, s_i, and o^g. To clearly illustrate the influence of the MC's locations on the power received by s_i, we refer to Fig. 3. In this figure, we can see a group of orange constructive curves between s_i and o^g. If the MC stays at any point on a constructive curve, the direct wave from MC and the reflected wave from o^g will completely constructively interfere at s_i, significantly enhancing its received power. Surrounding each constructive curve is a constructive area. When the MC stays within it, the power obtained by s_i can also be enhanced to a certain extent. Conversely, there is another group of blue destructive curves between s_i and o^g. If the MC is scheduled to any point on these curves, the multipath effects will notably weaken the power at s_i.

For the scenario where the combined power received by sensor s_i comprises direct waves from the MC and reflected waves from m environmental objects, we can express the amplitude of the combined power received by s_i as:

$$\begin{aligned} &A_{s_i}(t) = A_{C,s_i}(t) + \sum_{1\le g\le m} A_{o^g,s_i}(t) \\ &= \frac{A_0}{\hat{d}_{C,s_i}} \cos(\phi_0 + 2\pi(f t - \frac{d_{C,s_i}}{\lambda})) \\ &- \sum_{1\le g\le m} \frac{\Gamma^g A_0}{\hat{d}_{C,o^g}\hat{d}_{o^g,s_i}} \cos\left(\phi_0 + 2\pi\left(f t - \frac{(d_{C,o^g} + d_{o^g,s_i})}{\lambda}\right)\right). \end{aligned} \tag{7}$$

Similar to (6), the average combined power received by s_i is also obtained by calculating the ratio of the amplitude of the combined wave at s_i over one period to the duration of the period. Thus, the average combined power at s_i is:

$$\begin{aligned} P_{s_i} &= \frac{1}{T}\int_{-\frac{T}{2}}^{\frac{T}{2}} [A_{s_i}(t)]^2 \mathrm{d}t \\ &= \frac{A_0^2}{2\hat{d}^2_{C,s_i}} + \sum_{1\le g,q\le m}\left(-\frac{\Gamma^g A_0^2}{\hat{d}_{C,s_i}\hat{d}_{C,o^g}\hat{d}_{o^g,s_i}} \cos\frac{2\pi}{\lambda}(\triangle d_1)\right. \\ &\left. + \frac{\Gamma^g\Gamma^q A_0^2}{2\hat{d}_{C,o^g}\hat{d}_{o^g,s_i}\hat{d}_{C,o^q}\hat{d}_{o^q,s_i}} \cos\frac{2\pi}{\lambda}(\triangle d_2)\right). \end{aligned} \tag{8}$$

For simplicity, we use $\triangle d_1$ to represent the path difference between the direct wave from MC and the reflected wave from

object o^g (*i.e.*, $\triangle d_1 = d_{C,o^g} + d_{o^g,s_i} - d_{C,s_i}$), and $\triangle d_2$ to represent the path difference between the reflected wave from o^g and the reflected wave from another environmental object o^q (*i.e.*, $\triangle d_2 = d_{C,o^g} + d_{o^g,s_i} - d_{C,o^q} - d_{o^q,s_i}$). From (8), it is obvious that the power distribution involving multiple environmental objects is highly complex. Specifically, the relationships among the distances between the environmental objects, the MC, and s_i, along with the reflection coefficients of the environmental objects, collectively determine the power received by s_i.

In scenarios where an environmental object o^g is positioned between the MC and s_i, part of the waves emitted by the MC will be reflected by o^g while the remainder passes through it with attenuation, emerging on the opposite side with reduced amplitude. In this work, we introduce *shadow fading* [36] to characterize the blocking effect of environmental objects on radio waves. The following formula gives the power of a wave after penetrating an environmental object [25]:

$$P_{s_i} = \frac{\alpha P_0}{(d_{C,s_i} + \beta)^2} \times (1 - e^{-\sum_{g=1}^{G} \frac{1}{k_{o^g}}(1-\eta_{o^g})}), \quad (9)$$

where P_0 represents the transmission power of the MC. k_{o^g} denotes the traveling distance of the radio wave in the environmental object o^g, which depends on the relative positions of MC, sensor, and o^g. The coefficient η_{o^g} represents the wave penetration coefficient of the o^g. A value of $\eta_{o^g} = 1$ indicates that radio waves cannot penetrate the object, while $\eta_{o^g} < 1$ suggests partial penetration.

C. Cost Model

In one charging cycle, the energy consumption of the MC includes two parts: charging cost and traveling cost. Since P_0 is the transmission power of the MC, the charging cost is $P_0 \sum_{l_j \in L} \tau_{l_j}$, where L is the set of sojourn location, τ_{l_j} is the charging duration at sojourn location l_j. Assuming that e_{tr} and γ are the energy cost of the MC per unit distance and the total traveling distance in one charging cycle, respectively, the traveling cost is expressed as $e_{tr}\gamma$.

Thus, the total cost of the MC in one charging cycle is:

$$\mathcal{C} = P_0 \sum_{l_j \in L} \tau_{l_j} + e_{tr}\gamma. \quad (10)$$

D. Charging Utility Model

Limited by the sensor's electric circuits and the number of antenna coils, the power of radio waves received by sensors typically reaches a saturation state. This implies that the received power cannot exceed a certain threshold [24], [37]. We assume that there is a power threshold P_{th}. Then, we calculate the *charging utility* for a single sensor s_i as follows:

$$u(P_{s_i}) = \begin{cases} \frac{1}{P_{th}} \cdot P_{s_i}, & P_{s_i} < P_{th}, \\ 1, & P_{s_i} \geq P_{th}. \end{cases} \quad (11)$$

It can be seen that the normalized charging utility of s_i is initially proportional to its received power and then stabilizes at a constant value once the received power exceeds P_{th}. Then, for a sojourn location set $\mathcal{H}$ (which also represents the charging path) containing a limited number of sojourn locations, the overall charging utility is:

$$U(\mathcal{H}) = \sum_{l_j \in \mathcal{H}} u(l_j), \quad (12)$$

where, $u(l_j) = \sum_{s_i \in S_{l_j}} u(P_{s_i})$.

E. Problem Formulation

In this paper, we aim to design a charging scheduling scheme that utilizes the multipath effects resulting from the environmental objects to maximize the overall charging utility for all sensors in practical scenarios. Formally, we define the problem of charGing schEduling with mulTipath effectS (GETS) as follows:

$$(\mathbf{P1}) \qquad \text{maximize} \quad U(\mathcal{H}) = \sum_{l_j \in \mathcal{H}} u(l_j),$$
$$s.t.\, s_i \in S, l_j \in \Omega, s_i, l_j \notin o^g, \mathcal{C} \leq B. \quad (13)$$

III. Solution

In this section, to tackle the GETS problem, we first extract the Maximal Covering Sets (MCS) to determine the potential sojourn areas for the MC. Then, we divide each potential sojourn area into several subareas. Subsequently, by finding a local optimal position for each subarea, we identify a candidate sojourn location within each potential sojourn area. Finally, based on these candidate sojourn locations, we construct a shortest charging path that avoids environmental objects. Detailed methods for these processes are presented in the subsequent subsections.

A. Extracting Maximal Covering Sets and Corresponding Potential Sojourn Areas

In order to maximize the overall charging utility, the sojourn locations for MC should enable it to charge as many sensors as possible simultaneously. Due to geometric symmetry, no matter where the MC is located within a circle centered at a sensor with a radius equal to the longest charging distance D, the MC can charge the sensor. We extend this principle to all sensors in the network by drawing circles centered at sensors with a radius equal to D. If these circles overlap, it indicates that once the MC stays within the overlap, it can charge the corresponding sensors simultaneously.

Based on the sensor distribution in the network, we propose the following definition:

Definition 1: Maximal Covering Set (MCS): given a set of sensors S_{l_j} covered by the MC staying at sojourn location l_j, if there does not exist a sojourn location l_h where MC stays at such that $S_{l_h} \supset S_{l_j}$, S_{l_j} is called Maximal Covering Set.

Definition 2: Potential Sojourn Area: given an MCS, if there is an area, no matter where the MC stays within it, all sensors in the MCS can be charged by the MC, we refer to this area as the potential sojourn area of the MCS.

Fig. 4 depicts an example with two sensors, s_1 and s_2, along with an environmental object, o^g. It can be seen that the circles of s_1 and s_2 deformed due to the presence of o^g. When MC stays at

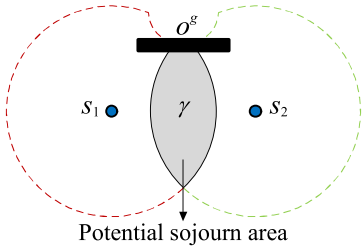

Fig. 4. Extracting MCS and corresponding potential sojourn area.

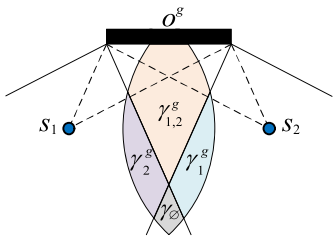

Fig. 5. Dividing the potential sojourn area.

any location within the overlap γ of these two deformed circles, it can simultaneously charge both sensors, s_1, s_2. Therefore, in Fig. 4, the MCS is s_1, s_2, and the corresponding potential sojourn area is γ.

B. Dividing the Potential Sojourn Areas

By extracting the MCSs, we can find out all the potential sojourn areas in the network. However, slight changes in the MC's location within each potential sojourn area may alter the number of the reflected waves received by each sensor in the corresponding MCS, resulting in variations in the number of constructive curves between sensors and environmental objects. This is due to the changes in the positional relationships between the MC and each sensor, as well as between the MC and nearby environmental objects. This variability in wave reception complicates the determination of a certain candidate sojourn location for the MC within each potential sojourn area. To address this challenge, we aim to divide each potential sojourn area into several types of subareas based on the positions of both the sensors and environmental objects. This division ensures that the number of constructive curve groups within each type of subarea is different.

In particular, based on the positional relationships between sensors and objects, potential sojourn area can be divided into the following four types of subareas:

Non-reflection Subarea is the subarea where no constructive curves exist. When the MC stays within a non-reflection subarea, all sensors in the corresponding MCS can not receive any reflected waves from environmental objects, only direct waves from the MC. For example, $\gamma_\varnothing$ in Fig. 5 is a non-reflection subarea. If the MC is scheduled to stay within it, sensors s_1 and s_2 can not receive any reflected wave from o^g.

1-Reflection Subarea is the subarea that contains at most one group of constructive curves. When the MC stays within a 1-reflection subarea, only one sensor in the corresponding MCS can receive a reflected wave from an environmental object. For instance, γ^g_1 in Fig. 5 is a 1-reflection subareas. If the MC is scheduled to stay within it, only s_2 can receive a reflected wave from o^g, which means that, at most, only one group of constructive curves may exist within this subarea. Similarly, γ^g_2 is also a 1-reflection subarea.

2-Reflection Subarea is the subarea that contains at most two groups of constructive curves. There are two possible situations when the MC stays within a 2-reflection subarea: one situation is that only one sensor in the corresponding MCS can receive reflected waves from two environmental objects, and the other situation is that two sensors in the corresponding MCS can receive reflected waves from one environmental object. For example, $\gamma^g_{1,2}$ in Fig. 5 is a 2-reflection subarea. If the MC is scheduled to stay within it, both sensors s_1 and s_2 can receive the reflected waves from o^g. This means that, at most, two groups of constructive curves exist within $\gamma^g_{1,2}$.

***m**-Reflection Subarea* is the subarea that may contain m $(m > 2)$ groups of constructive curves. For example, consider a subarea where the MC stays, and two sensors in the corresponding MCS can receive reflected waves from two nearby environmental objects. This subarea may contain at most four groups of constructive curves, making it a 4-reflection subarea.

For any MCS in the network, after dividing its potential sojourn area into four types of subareas, we aim to find the local optimal position within each subarea where the MC can maximize the overall power received by the sensors in the MCS. Then, we select the one among all local optimal positions as the candidate sojourn location of the MCS. The specific method for finding local optimal positions is detailed in the next subsection.

C. Finding the Candidate Sojourn Locations Within the Potential Sojourn Areas

After dividing a potential sojourn area, we obtain four types of subarea that contain corresponding groups of constructive curves. Considering the greater the number of groups of constructive curves, the more complex the power distribution within each subarea, we start by finding the local optimal position in the non-reflection subarea where no constructive curves exist. Then, we further explore the subareas that may contain different numbers of groups of constructive curves to identify the local optimal position within each subarea.

Case 1. Subarea is non-reflection Subarea:

In this case, we aim to find a local optimal position within a continuous non-reflection subarea, which implies an infinite number of positions. Therefore, we use multiple constant segments $\bar{P}(d)$ to approximate the direct power function $P(d)$. We properly control the number of the constant segments Q and the endpoints $z(0), \ldots, z(Q)$ $(z(0) = 0, z(Q) = D)$, ensuring that the approximation error for each constant segment is less than a given value. $\bar{P}(d)$ is defined as:

$$\bar{P}(d) = \begin{cases} P(z(1)), & d = z(0), \\ P(z(q)), & z(q-1) < d \le z(q) (q = 1, 2, \ldots, Q), \\ 0, & d > z(Q), \end{cases} \tag{14}$$

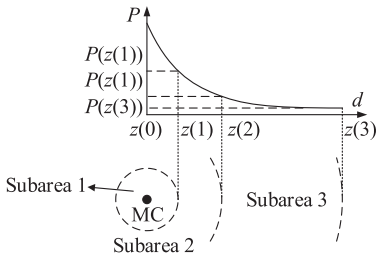

Fig. 6. Power approximation.

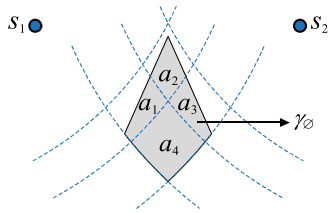

Fig. 7. Dividing non-reflection subarea $\gamma_\varnothing$ into four fine-grained regions.

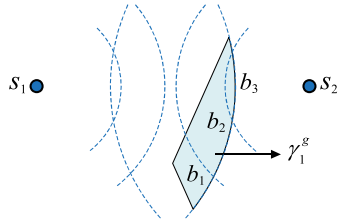

Fig. 8. Dividing 1-reflection subarea γ_1^g into three fine-grained regions.

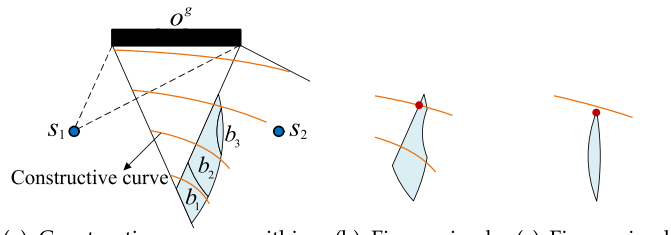

(a) Constructive curves within γ_1^g. (b) Fine-grained region b_2. (c) Fine-grained region b_3.

Fig. 9. Finding local optimal position within regions of 1-reflection subarea.

where $z(0) = 0$, $z(Q) = D$, and $z(q) = \beta((1+\varepsilon)^{\frac{q}{2}} - 1), q = 1, \ldots, Q-1$ ($Q = \lceil \frac{\ln[((D+\beta)/\beta)^2]}{\ln(1+\varepsilon)} \rceil$), ε is the predetermined approximation error threshold. Furthermore, we have the following theorem to bound ε.

Theorem 1: The approximation error ε in using $\bar{P}(d)$ to approximate $P(d)$ is subject to:

$$1 \leq \frac{P(d)}{\bar{P}(d)} \leq 1 + \varepsilon, d \leq D. \tag{15}$$

Fig. 6 illustrates the fundamental concept of approximating the power function received by the sensor from the MC. In this figure, the number of discrete levels Q is set to 3, $z(0)$, $z(1)$, $z(2)$, and $z(3)$ represent the endpoints of the Q constant segments. The charging range of the MC is discretized into three subareas, subarea 1, subarea 2, and subarea 3. Within each subarea, the received power is approximated as constants $P(z(1))$, $P(z(2))$, and $P(z(3))$, respectively, regardless of the sensor's exact position. It is evident that increasing Q results in a finer discretization of the charging region into a greater number of subareas, thereby reducing the approximation error and improving the accuracy of the power approximation.

After discretization, we select the fine-grained region that the MC stays could yield the maximum total charging power received by surrounding sensors, and randomly choose a position within as the local optimal position. As depicted in Fig. 7, subarea $\gamma_\varnothing$ is discretized into four fine-grained regions: a_1, a_2, a_3 and a_4, according to the piecewise constant function $\bar{P}(d)$. Within each fine-grained region, the powers from the MC at sensors s_1 and s_2 remain approximately constant, regardless of the MC's exact location. Obviously, the fine-grained region a_2, where the MC stays, could yield the maximum total received charging power, indicating that the MC's stay at a_2 would result in the maximal total charging utility. Therefore, we randomly choose a position within it as the local optimal position of $\gamma_\varnothing$.

Case 2. Subarea is a 1-Reflection Subarea:

In this case, the MC staying within a 1-reflection subarea only enables one sensor in the MCS to receive reflected waves from one environmental object. To find the local optimal positions in 1-reflection subareas, we need to jointly consider the power of the combined wave received by this sensor and the power of the direct waves received by the other sensors.

Similar to the non-reflection subarea, we first use the piecewise constant function $\bar{P}(d)$ to discretize the 1-reflection subareas into several fine-grained regions. Thus, for each fine-grained region, the power of the direct waves from the MC received by the sensors in the corresponding MCS can be regarded as constant within a predetermined error threshold ε. For instance, in Fig. 8, 1-reflection subarea γ_1^g is discretized into three fine-grained regions b_1, b_2 and b_3, where the MC staying within each region, the powers of the direct waves at s_1 and s_2 are constant, respectively

Moreover, for the only sensor that receives reflected wave from the environmental object, the specific location of the MC within each fine-grained region determines the power of the combined wave at it. Therefore, we focus on finding the local optimal position on the constructive curves that will enhance the combined power at the sensor. Depending on whether there is a constructive curve in each fine-grained region, there are 2 different situations to consider in finding the candidate local position: (1) the fine-grained regions contain constructive curves (see b_1 and b_2 in Fig. 9(a)); (2) the fine-grained regions do not contain constructive curves (see b_3 in Fig. 9(a)).

For the fine-grained regions that contain constructive curves, the position closest to the environmental object on the curves is the candidate local position (see the red dot in Fig. 9(b)). The rationale is that the higher the power of the reflected wave involved in the interference, the higher the combined power received by the sensor.

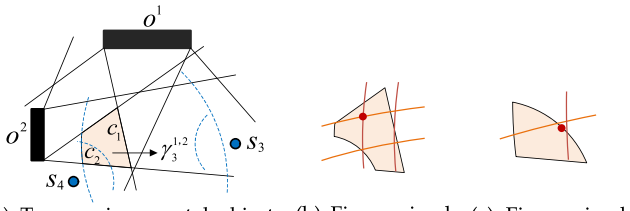

(a) Two environmental objects yielding a 2-reflection subarea. (b) Fine-grained region c_1. (c) Fine-grained region c_2.

Fig. 10. Finding local optimal position within regions of 2-reflection subarea.

For the fine-grained regions that contain no constructive curves, the position closest to the nearest constructive curve within the subarea is the candidate local position (see the red dot in Fig. 9(c)). This is because it is the most likely position for constructive interference between reflected waves and direct waves at the sensor.

After identifying all candidate local positions within the 1-reflection subarea, we calculate the total charging utility at each position. Among these candidates, we select the position that yields the maximum charging utility as the local optimal position.

Case 3. Subarea is 2-Reflection Subarea:

In this case, we also first discretize the subarea into several fine-grained regions where the MC staying enables sensors in the corresponding MCS to receive a constant power of the direct waves from it.

Before presenting our approach to finding the candidate local position in each fine-grained region, we would like to point out that two scenarios can form the 2-reflection subareas: (1) one environmental object is near two sensors (see γ_1^g in Fig. 5); (2) two environmental objects are near one sensor (see $\gamma_3^{1,2}$ Fig. 10(a)). Intuitively, finding the local optimal position within a 2-reflection subarea is more challenging than within a 1-reflection subarea, especially in scenarios with two environmental objects. In such a scenario involving multiple environmental objects, the wave emitted by the MC may undergo multiple reflections between these objects. However, with each propagation and reflection, the intensity of the wave attenuates significantly and becomes very weak after multiple reflections. Taking this into account and following [38], we ignore the waves that are reflected multiple times between environmental objects.

Thus, the core concept behind determining the local optimal position within the 2-reflection subareas is to concentrate on the intersections of the constructive interference curves generated by the waves from the MC and the primary reflected waves. For clarity, the term "reflected wave" in the subsequent discussion specifically refers to the primary reflected wave.

The reason behind this is that when the MC stays at an intersection of constructive curves, for the scenario with one environmental object, the direct waves and the reflected waves constructively interfere at the two sensors simultaneously; for the scenario with two environmental objects, the direct waves and the reflected waves from different objects constructively interfere at the sensor at the same time.

In particular, based on whether there is an intersection of constructive curves in each fine-grained region, there are 2 different situations to consider in finding the candidate local positions: (1) the fine-grained regions contain the intersection of constructive curves; (2) the fine-grained regions do not contain the intersection of constructive curves;

In the first situation, we need to compare all intersections, and the one that can yield the maximum total power received by surrounding sensors will be identified as the candidate local position (see red dots in Fig. 10(b)).

In the second situation, we choose the position closest to the nearest intersection as the candidate local position within it (see red dot in Fig. 10(c)). The reason behind this is the closer the MC is to the intersection, the more likely the direct waves will completely constructively interfere with the reflected waves at the corresponding sensors.

After identifying all the candidate local positions in the 2-reflection subarea, we select the one with the maximum total charging utility among them as the local optimal position.

Case 4. Subarea is m -Reflection Subarea:

In scenarios where multiple environmental objects are located near several sensors, *m*-reflection subareas $(m > 2)$ may emerge. Notably, a large number of environmental objects will yield a series of different *m*-reflection subareas and there are many constructive curves within each *m*-reflection subarea. Consequently, identifying each local optimal position from the intersections of the constructive curves within each *m*-reflection subarea will result in very high computational complexity.

Note that, in real-world scenarios, the distance between each environmental object and each sensor, as well as the reflection coefficient of each object, will be various. As a result, the intensity of the reflected waves propagating at each sensor will be different. Obviously, reflected waves with lower intensities have a diminished impact on the combined power received by the sensor. To address the computational challenges posed by complex environments, a more efficient strategy is to prioritize high-intensity reflected waves. Specifically, we select the strongest n reflected waves and determine the local optimal position of the m-reflection subareas by finding the intersection points of the corresponding constructive curves. It is evident that a larger value of n allows for the constructive interference of more reflected waves with the waves from the MC at the sensor, enhancing the overall charging utility. However, this comes at the cost of higher computational complexity. Conversely, a smaller value of n improves computational efficiency but may not fully capture the benefits of all reflected waves. In Section V-D, we conduct field experiments in the scenario with multiple environmental objects to validate the effectiveness of our approach. The results verify that only considering the reflected waves from 2 or 3 environmental objects could significantly improve the charging performance while considering more environmental objects has a minimal effect on further performance improvement.

After determining the local optimal position within each subarea of a potential sojourn area, we select the position with the highest total charging utility as the candidate sojourn location for the corresponding MCS. This position is then added to the candidate sojourn location set L to construct the charging path.

D. Constructing Charging Path With Environmental Objects

Since the battery capacity B of the MC is limited, it may not be able to visit all candidate sojourn locations. Additionally, environmental objects may obstruct the paths between certain sojourn locations. Therefore, we reformulate our GETS problem as: how to select a subset of candidate sojourn locations to construct the shortest charging path $\mathcal{H}$ to maximize the overall charging utility $U(\mathcal{H})$, under the constraint of limited battery capacity of the MC.

$$(\mathbf{P2}) \quad \text{maximize} \quad U(\mathcal{H}) = \sum_{l_j \in \mathcal{H}} u(l_j),$$
$$\text{s.t.}\, s_i \in S, l_j \in \mathcal{H}, s_i, l_j \notin o^g,$$
$$\mathcal{H} \subseteq L, \mathcal{C} \leq B. \tag{16}$$

Definition 3: (Nonnegativity, Monotonicity, and Submodularity). Given a non-empty finite set S, and a function f defined on the power set 2^S of S with real values. f is called nonnegative, monotone, and submodular if and only if it satisfies the following conditions, respectively:

- Nonnegativity: $f(\emptyset) = 0$ and for any $X \subseteq S$, $f(X) \geq 0$.
- Monotonicity: for all $X \subseteq Y \subseteq S$, $f(X) \leq f(Y)$; or for any $X \subseteq S$ and $e \in S \backslash X$, $f(X \cap e) - f(X) \geq 0$.
- Submodularity: for any $X \subseteq Y \subseteq S$ and $e \in S \backslash Y$, $f(X \cap \{e\}) - f(X) \geq f(Y \cap \{e\} - f(Y)$.

Theorem 2: The objective function $U(\mathcal{H})$ is nonnegative, monotone, and submodular.

Proof: To verify whether the $U(\mathcal{H})$ is a submodular function, we need to prove that $U(\mathcal{H})$ satisfies the conditions in Definition 3.

1. According to (11) and (12), it is evident that $U(\emptyset) = 0$, as there are no sojourn locations for the MC to stop and charge the sensors. Only when there is at least one sojourn location for the MC to charge the sensors does the charging utility become greater than zero. Therefore, for $X' \neq \emptyset$, $U(X') > 0$, indicating that $U(\mathcal{H})$ is nonnegative.
2. It is also evident that adding a new sojourn location to the charging path increases the overall charging utility, as defined by $U(\mathcal{H})$ in (12). Given a virtual charging path $X' \subseteq X$, we have:
$$U(X') \leq U(X), \tag{17}$$
which confirms that the function $U(\mathcal{H})$ is monotone.
3. For any sojourn location sets $X' \subseteq X \subseteq S$, we aim to prove that
$$U(X' \cup l) - U(X') \geq U(X \cup l) - U(X), \quad l \in S \backslash X. \tag{18}$$
From (12), we observe that $U(\mathcal{H})$ is an increasing function because adding more sojourn locations provides higher charging utility. Therefore, we have:
$$U(X' \cup l) - U(X') = U(X \cup l) - U(X) = U(l). \tag{19}$$
Thus, the function $U(\mathcal{H})$ is submodular.

Then, $U(\mathcal{H})$ is proved to be nonnegative, monotone, and submodular. □

Due to the properties of our objective function, we adopt a greedy-based strategy to construct the charging path. The basic idea is: we greedily select a candidate sojourn location belonging to the candidate sojourn location set that can maximize the utility-cost ratio in each iteration:

$$l_j^* = \arg \max_{l_j \in L \backslash \mathcal{H}} \frac{U(\mathcal{H} \cup \{l_j\}) - U(\mathcal{H})}{\mathcal{C}(\mathcal{H} \cup \{l_j\}) - \mathcal{C}(\mathcal{H})}, \tag{20}$$

where L is the set of the candidate sojourn locations that have not been added to the charging path, and $\mathcal{H}$ represents the set of sojourn locations in the path. $U(\mathcal{H} \cup \{l_j\}) - U(\mathcal{H})$ represents the charging utility benefit gained by adding l_j, $\mathcal{C}(\mathcal{H} \cup \{l_j\}) - \mathcal{C}(\mathcal{H})$ the corresponding increase in battery consumption.

After a new sojourn location is selected, we use the Obstacle Avoidance (OA) algorithm [26] to calculate the distance between it and other sojourn locations as well as the BS without crossing any environmental objects. Then, we construct an initial shortest charging path that includes the selected sojourn locations by using the nearest neighbor rule [39] to approximate the travel cost. Through continuous iteration, until the residual battery of the MC cannot support serving more sojourn locations, the shortest charging path that can avoid obstacles can be obtained.

Theorem 3: With a slightly relaxed budget, our scheme is better than $\frac{1}{2}(1 - e^{-1})$ of the optimal solution to the GETS problem.

Proof: First, in Algorithm 1, we use discretization to discrete the sojourn area for MC, according to Theorem 1, (11) and (12), the **P2** problem can be reformulated as:

$$(\mathbf{P3}) \quad \text{maximize} \quad U(\mathcal{H}) = \sum_{l_j \in \mathcal{H}} u(l_j) = \sum_{l_j \in \mathcal{H}} \sum_{s_i \in S_{l_j}} \bar{P}(d),$$
$$s.t.\, s_i \in S, l_j \in \Omega, s_i, l_j \notin o^g, \mathcal{C} \leq B. \tag{21}$$

Suppose the optimal solution achieves the maximum power, then we have $P_{opt} = P(d)$, according to Theorem 1. Thus, we derive $\bar{P}(d) \geq P(d) \cdot \frac{1}{1+\varepsilon}$, indicating that the total charging time for our scheme is no longer than $\frac{1}{1+\varepsilon}$ times the optimal charging time. Consequently, the charging cost incurred by our scheme does not exceed $\frac{1}{1+\varepsilon}$ of the optimal charging cost.

Since the nearest-neighbor strategy is used to construct the charging path and it has been proven to yield a path length shorter than $\frac{1}{2}\lceil \lg(n) \rceil + \frac{1}{2}$ times the optimal path length [39]. As the traveling cost is proportional to the charging path length, the traveling cost of our scheme is guaranteed to be lower than $\frac{1}{2}\lceil \lg(n) \rceil + \frac{1}{2}$ times the optimal traveling cost.

Therefore, the overall approximation ratio of our scheme is $\max\{(1+\varepsilon)^{-1}, \frac{1}{2}\lceil \lg(n) \rceil + \frac{1}{2}\}$.

According to [40], with a slightly relaxed budget $\frac{\alpha(1+\alpha(K_c-1)(1-k_c))}{\max(1+\varepsilon)^{-1}, \frac{1}{2}\lceil \lg(n) \rceil + \frac{1}{2}K_c} B$, our scheme achieves an approximation ratio of $\frac{1}{2}(1 - e^{-1})$ of the optimal solution.

Here, α is defined as $\alpha = \min_x \min_{A,\, B: A \subseteq B} \frac{C(x|A)}{C(x|B)}$, where k_c represents the total curvature of a submodular function, given by $k_c = 1 - \min_{l_j \in \mathcal{H}} \frac{C(l_j|\mathcal{H} \backslash l_j)}{C(l_j)}$, and K_c is the maximum cardinality of $\mathcal{H}$ satisfying $\mathcal{C} \leq B$. □

TABLE II
SIMULATION PARAMETERS

Parameters	Default values
Number of sensors around a PoI	$2 \sim 5$
Number of objects around a PoI	$1 \sim 4$
Energy consumption rate (v)	$[0.5mJ, 2mJ]$
Transmission power (P_0)	$1W \sim 5W$
Wavelength (λ)	$0.328m$
Upper-bound receiving power (P_{th})	$20mW$
Battery capacity of sensor (b)	$50J$

IV. SIMULATIONS

In this section, we conduct simulations to evaluate the performance of our GETS scheme on different sojourn locations with various environmental objects.

A. Simulation Setup

In simulations, we randomly deploy 2-5 sensors around a PoI (Point of Interest), each with a battery capacity of $50J$. Additionally, 1-4 environmental objects made of different materials (*i.e.*, wood, brick, and metal) and shapes (*i.e.*, cylindrical and rectangular) are randomly distributed around the sensors. The reflection coefficients of wood, brick, and metal are set to 0.1, 0.5, and 0.98, respectively [41]. The MC's transmission power P_0 is set to 3 W, and its wavelength is set as 32.8 cm, according to the commodity off-the-shelf TX91501 wireless charger produced by Powercast [28]. The other parameters used in our simulations are set as $\alpha = 9.5$, $\beta = 6$, $\varepsilon = 0.2$, and $P_{th} = 20$ mW. All simulation results are the average values from 100 trials with random sensor deployments and environmental object distributions. Table II lists the parameters used in the simulation, which will be applied as the default settings unless stated otherwise.

To evaluate the effectiveness of the GETS scheme, we compare it with the following three charging algorithms:

Maximized charging utility with Constructive Curves (MCC) is a charging algorithm that considers the multipath effects. After discretizing the potential charging area into several subareas, MCC selects the subarea that could maximize the additive power of the surrounding sensors then identifies the position on the constructive curves that can generate the strongest reflection wave and schedules the MC to stay at this position.

Maximized charging utility with Blocking Esffects (MBE) [25] is a charging algorithm that considers the blocking effects of environmental objects on waves but does not account for the multipath effects.

Maximized charging utility with Wave Reflection (MWR) [27] is a charging algorithm that leverages wave reflection to extend the charging range of the MC, enabling both line-of-sight and non-line-of-sight charging. It is important to note that MWR does not account for the multipath effects induced by wave reflection during the charging process.

Randomized Sojourn Location (RSL) randomly chooses a position within the potential sojourn area as the sojourn location of the MC.

B. Performance Comparisons

In this subsection, the default number of sensors is set to 2, and the default number of environmental objects is set to 1, with the material being metal.

Impact of number of sensors N : The simulation results show that, on average, GETS outperforms MCC, MBE, MWR, and RSL by 13.62% , 23.18% , 22.92% , and 95.72% , respectively, in terms of *N*. As shown in Fig. 11(a), GETS achieves the highest overall charging utility. This is because it carefully selects the sojourn location for the MC to ensure that the reflected waves and the direct waves constructively interfere at sensors. Furthermore, since the MCC algorithm considers the multipath effects, it performs better than MBE, MWR and RSL.

Impact of number of environmental objects M: The simulation results show that, on average, GETS outperforms MCC, MBE, MWR, and RSL by 10.05% , 19.96% , 20.26% , and 92.78% , respectively, in terms of *M*. As illustrated in Fig. 11(b), the overall charging utility achieved by GETS slightly increases with the number of environmental objects. This demonstrates that our GETS scheme can effectively leverage varying numbers of environmental objects to enhance charging performance and remain robust across different charging environments.

Impact of object's materials: The simulation results show that, on average, GETS outperforms MCC, MBE, MWR, and RSL by 9.4% , 22.7% , 21.25% , and 98.21% , respectively, in terms of the materials of the objects. From Fig. 11(c), we can observe that since the environmental objects with higher reflection coefficients generate stronger reflected waves, our GETS scheme performs better when the environmental object is made of metal compared to other materials, and its advantage over the other three algorithms is even greater.

Impact of transmission power P_0: The simulation results show that, on average, our algorithm GETS outperforms MCC, MBE, MWR, and RSL by 20.21% , 41.94% , 42.69% , and 108.19% , respectively, in terms of P_0. It can be seen from Fig. 11(d) that the overall charging utilities achieved by all the algorithms increase with P_0. Our GETS scheme consistently demonstrates superior performance, which verifies its suitability to WRSNs employed with different chargers.

V. FIELD EXPERIMENTS

To further verify the effectiveness of our GETS scheme in practical applications, we first conduct outdoor field experiments, followed by indoor field experiments. Finally, we verify the adaptability of our scheme to complex environments in scenarios involving multiple environmental objects.

A. Testbed

Our testbed consists of an MC equipped with a TX91501 wireless power transmitter and a battery with a capacity of 2,000 KJ [11], 8 rechargeable sensors with a capacity of $50J$,

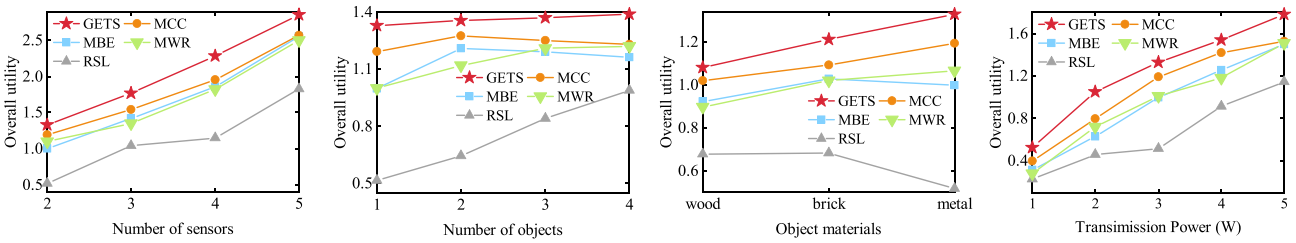

(a) N vs. overall charging utility. (b) M vs. overall charging utility. (c) Materials vs. charging utility. (d) P_0 vs. overall charging utility.

Fig. 11. Simulation results.

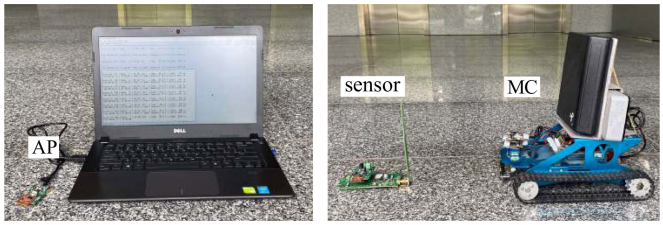

Fig. 12. Testbed.

TABLE III
FIELD EXPERIMENT PARAMETERS

Parameters	Default values
Number of sensors	8
Moving cost of MC	$50J/m$
Transmission power (P_0)	$3W$
Battery capacity of sensor (b)	$50J$
Battery capacity of MC (B)	$2,000KJ$

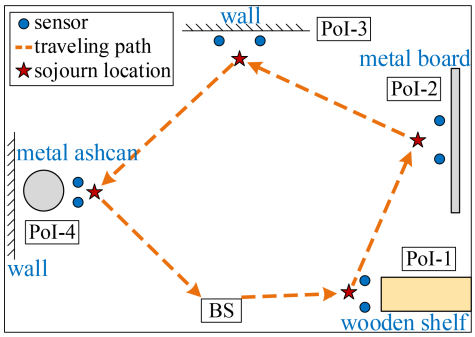

Fig. 13. Diagram of indoor experimental fields.

an AP connected to a laptop to collect information delivered by the sensors, as shown in Fig. 12. The moving cost of the MC is 50 J/m [11]. All the power transmitters, sensors, and AP are produced by Powercast [28]. We list all the parameters in Table III, which will be applied as the default settings unless stated otherwise.

B. Indoor Experiments

We conduct indoor experiments in the hall of a teaching building, with dimensions of 5 m $*$ 7 m. As shown in Fig. 13,

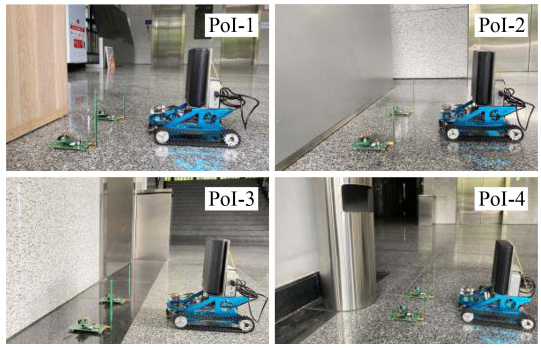

Fig. 14. 4 PoIs of indoor experiments.

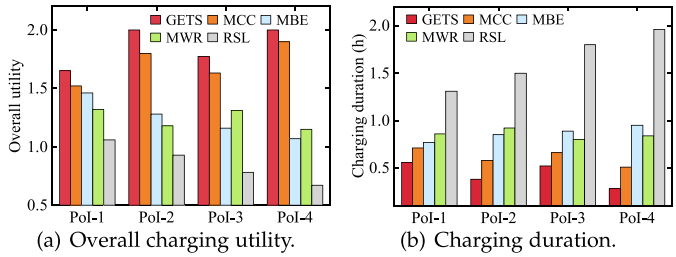

Fig. 15. The indoor experiment results.

the charging path includes four Points of Interests (PoIs), and the total length of the path is 9.4 m. For each PoI, we placed two sensors to monitor temperature, humidity, and other environmental information. These PoIs are located as follows: PoI-1 is near a wooden bookshelf. PoI-2 is near a metal board. PoI-3 is situated adjacent to a wall. PoI-4 is placed next to a metal ashcan and a wall, as depicted in Fig. 14.

Fig. 15(a) shows the results of the charging utility achieved by the four algorithms at each PoI. On average, GETS outperforms MCC, MBE, MWR, and RSL by 8.38% , 52.19% , 50.88% , and 124.04% , respectively. It also can be seen that the GETS and MCC, which consider multipath effects, have relatively greater advantages at PoI-2 and PoI-4, where metal environmental objects are distributed.

Fig. 15(b) presents the results of the charging duration for each PoI obtained by the four algorithms. On average, the GETS scheme reduces charging duration by 30.48% , 48.67% , 48.81% , and 72.19% , respectively, compared to MCC, MBE, MWR, and RSL. This verifies that using our GETS scheme in indoor scenarios can effectively reduce the charging duration.

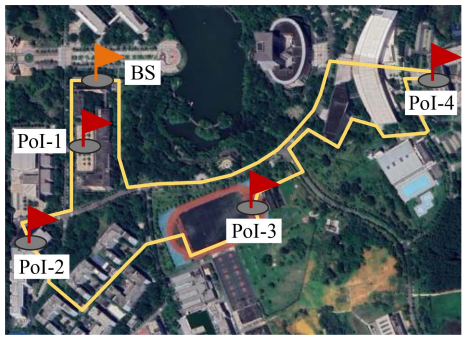

Fig. 16. Diagram of outdoor experimental fields.

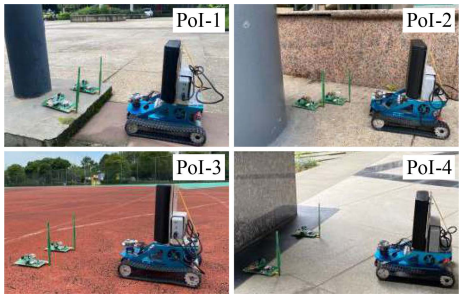

Fig. 17. 4 PoIs of outdoor experiments.

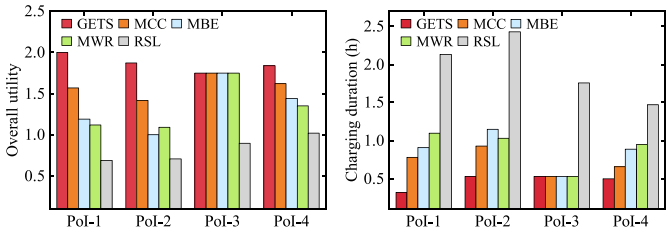

Fig. 18. The outdoor experiment results.

C. Outdoor Experiments

We also conduct outdoor experiments in various scenarios across a university campus. As shown in Fig. 16, an MC starts from a Base Station (BS) to visit the four PoIs to charge surrounding sensors sequentially, then return to the BS before exhausting its energy. Similar to indoor experiments, we placed two sensors around each PoI, the specific situations of these four PoIs are shown in Fig. 17: PoI-1 is positioned adjacent to a metal lamp post. PoI-2 is near a cylinder pillar and stairs. PoI-3 is on an empty playground. PoI-4 is near a square pillar. The total length of the charging path is 2.46 km.

Fig. 18(a) compares the charging utility yielded by the four algorithms. On average, GETS outperforms MCC, MBE, MWR, and RSL by 18.16% , 45.71% , 46.61% , and 132.02% , respectively. It can be seen that, except for the PoI-3, which has no environmental objects nearby, the GETS scheme achieves the best performance regardless of the number of environmental objects (whether 1 or 2), their material, or their size near the other PoIs.

Fig. 18(b) compares the charging duration obtained by the four algorithms at each PoI. On average, compared to MCC, MBE, MWR, and RSL, GETS reduces the charging duration by 31.57% , 40.64% , 41.71% , and 75.08% , respectively. Similar to indoor experiments, our GETS scheme still achieved the shortest charging duration.

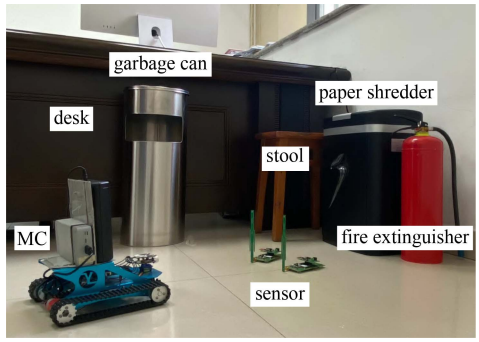

Fig. 19. Multiple objects experiment.

D. Multiple Environmental Objects Experiments

To validate the proposed method for determining the candidate sojourn location in scenarios where multiple environmental objects are located near several sensors (see **Case 4** in Section III-C), a field experiment is conducted.

As shown in Fig. 19, a PoI with two sensors is surrounded by various environmental objects, including a metal garbage can, a metal fire extinguisher, a plastic paper shredder, a wooden stool, and a wooden desk. Two sensors are positioned near the PoI to monitor environmental parameters such as temperature, humidity, and other related data.

First, we determine the MC's sojourn location without considering any environmental objects as a baseline. Next, we include the metal garbage can, which has the highest reflection coefficient and is positioned closer to the sensors than the other environmental objects, to refine the sojourn location. Finally, we incrementally add one environmental object at a time, prioritizing those with higher reflection coefficients and closer proximity to the sensors, until all environmental objects are considered.

The results of the charging utility under varying numbers of considered environmental objects are shown in Fig. 20. It can be observed that the overall charging utility increases rapidly at the beginning and gradually stabilizes. This confirms that, in this experimental scenario, considering two environmental objects that generate strong reflected waves (e.g., a metal garbage can and a metal fire extinguisher) can significantly enhance the power intensity received by sensors, while taking more environmental objects into account and contribute very little to further improving charging efficiency. Thus, we can conclude that applying our GETS scheme in complex scenarios can achieve satisfactory charging performance while maintaining low computational complexity.

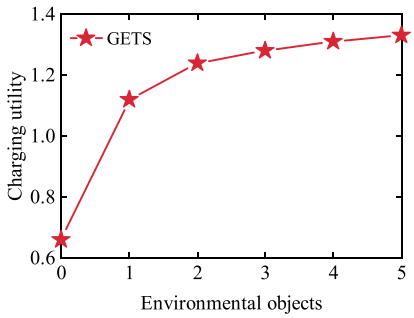

Fig. 20. The multiple objects experiment.

VI. Related Work

In this section, we provide a review of the existing literature on charging scheduling strategies and wireless charging techniques in the presence of environmental objects.

A. Charging Scheduling

In the field of mobile charging, many scheduling schemes have been proposed. Lin et al. [42] developed a directional charging scheme aimed at minimizing charging delays. They enhanced the energy transfer model by introducing linear constraints and designed an approximation algorithm to address the problem of charging delay minimization. In [6], Liu et al. devised a charging scheduling algorithm based on reinforcement learning to charge mobile devices with non-deterministic mobility. Ren et al. [11] observed energy leaking behind the directional charger. To make full use of this part of the energy, the authors built a charging model considering the back lobe of the charger and proposed a charging scheduling scheme to minimize the number of dead sensors and maximize energy usage effectiveness. Sun et al. [17] investigated the impact of dynamic environments where sensor locations drift randomly within a certain range. Recognizing that location deviations exhibit distinct behaviors over short and long terms, they noted that relying solely on long-term expectations could significantly reduce charging efficiency in the short term. Huang et al. [21] considered the unpredictable events in dynamic networks and designed an adaptive charging scheme with a rapid data-sharing protocol for the network with varying energy consumption. To avoid the unpredictable events-induced cumulative change that may cause the deaths of some sensors, they designed a mobile adaptive charging scheme with a rapid data-sharing protocol for WRNs with varying energy consumption. In [43], Wu et al. explored cooperative scheduling for directional charging considering spatial occupation and proposed an approximation algorithm to minimize the overall charging cost. Lin et al. [44] proposed a cost-efficient approximation algorithm to maximize charged energy in a 3-D WRSN with energy constraints where a UAV is employed for energy replenishment. In [45], Sun et al. jointly scheduled the MCs freeloading or executing charging tasks to improve the energy efficiency of the whole network.

Although these studies have explored efficient mobile charging strategies across various scenarios, they have overlooked the multipath effects induced by ubiquitous environmental objects in real-world applications. This omission leads to two limitations. First, the absence of multipath considerations results in a significant discrepancy between the theoretically expected power received by the sensor and the actual power it obtains when the proposed charging scheduling schemes are deployed. This discrepancy can degrade charging efficiency and overall network performance. Second, existing approaches fail to leverage the constructive interference of waves propagating along multiple paths, which could otherwise be exploited to enhance the charging utility of the network.

B. Environmental Objects Issue in Wireless Charging

Recently, a few pioneering researchers have begun to focus on the impact of environmental objects on the charging process. In [24], Wang et al. noticed that objects can block the transmission of radio waves so that sensors located between objects and chargers can not receive any power. Based on this premise, they proposed a charger deployment scheme aimed at maximizing charging utility. You et al. [25], demonstrated that radio waves can penetrate various objects with different attenuation coefficients. They designed a charger deployment scheme to maximize overall charging utility in scenarios where sensors are distributed on a 2D plane with obstacles of arbitrary shapes and materials. In [46], [47], Lin et al. concentrated on how to utilize the wave diffraction caused by environmental objects. They proposed a charging scheme based on the Fresnel model to maximize charging utility. Yang et al. [27], considered wave reflection on environmental objects and proposed a charging scheduling scheme that adapts to both line-of-sight and non-line-of-sight charging by leveraging wave reflections.

While these studies have begun to consider environmental objects, their understanding of their impact on the actual power received by sensors remains incomplete. They overlooked the multipath effects resulting from wave reflections by environmental objects, which hinder the sensors from achieving the maximum possible charging utility through constructive wave interference. This oversight has prevented them from fully utilizing ubiquitous environmental objects to improve charging performance.

VII. Conclusion

In this paper, we focus on designing a charging scheduling scheme that leverages the multipath effects induced by environmental objects. First, we build a charging model that considers multipath effects to investigate power distribution within a practical charging scenario. Then, based on this model, we propose a scheme that determines the sojourn locations and constructs a charging tour avoiding obstacles, achieving a $\frac{1}{2}(1-e^{-1})$ approximation ratio to the optimal solution with a slightly relaxed budget. Extensive simulations and field experiments demonstrate the superior performance of our scheme in several real-world scenarios.

REFERENCES

[1] A. Kurs, A. Karalis, R. Moffatt, J. D. Joannopoulos, P. Fisher, and M. Soljacic, "Wireless power transfer via strongly coupled magnetic resonances," *Science*, vol. 317, no. 5834, pp. 83–86, 2007.

[2] WPC, Wireless power consortium, 2025. [Online]. Available: https://www.wirelesspowerconsortium.com/

[3] NMSC, Wireless charging market by technology and industry vertical–global opportunity analysis and industry forecast 2024–2030. [Online]. Available: https://www.nextmsc.com/report/wireless-charging-market

[4] X. Fan et al., "Towards flexible wireless charging for medical implants using distributed antenna system," in *Proc. ACM Annu. Int. Conf. Mobile Comput. Netw.*, 2020, pp. 1–15.

[5] S. He, K. Hu, S. Li, L. Fu, C. Gu, and J. Chen, "A robust RF-based wireless charging system for dockless bike-sharing," *IEEE Trans. Mobile Comput.*, vol. 23, no. 3, pp. 2395–2406, Mar. 2024.

[6] T. Liu, B. Wu, W. Xu, X. Cao, J. Peng, and H. Wu, "RLC: A reinforcement learning-based charging algorithm for mobile devices," *ACM Trans. Sensor Netw.*, vol. 17, no. 4, pp. 1–23, 2021.

[7] P. Zhou, C. Wang, and Y. Yang, "Design of self-sustainable wireless sensor networks with energy harvesting and wireless charging," *ACM Trans. Sensor Netw.*, vol. 17, no. 4, pp. 1–38, 2021.

[8] W. Zhou, X. Wang, H. Zhou, S. Jiang, Z. Liu, and Y. Ji, "Safety Guaranteed Power-Delivered-to-Load Maximization for Magnetic Wireless Power Transfer," in *Proc. IEEE Int. Conf. Comput. Commun.*, 2024, pp. 2049–2058.

[9] Y. Ma, D. Wu, J. Gao, W. Sun, J. Yang, and T. Liu, "Dynamic power distribution controlling for directional chargers," in *Proc. IEEE Int. Conf. Comput. Commun.*, 2024, pp. 2059–2068.

[10] M. Ren et al., "Understanding wireless charger networks: Concepts, current research, and future directions," *IEEE Commun. Surveys Tuts.*, early access, Oct. 28, 2024, doi: 10.1109/COMST.2024.3486820.

[11] M. Ren, D. Wu, J. Xue, W. Xu, J. Peng, and T. Liu, "Utilizing the neglected back lobe for mobile charging," in *Proc. IEEE Int. Conf. Comput. Commun.*, 2023, pp. 1–10.

[12] Y. Sun et al., "Trading off charging and sensing for stochastic events monitoring in WRSNs," *IEEE/ACM Trans. Netw.*, vol. 30, no. 2, pp. 557–571, Apr. 2022.

[13] W. Xu, W. Liang, X. Jia, H. Kan, Y. Xu, and X. Zhang, "Minimizing the maximum charging delay of multiple mobile chargers under the multi-node energy charging scheme," *IEEE Trans. Mobile Comput.*, vol. 20, no. 5, pp. 1846–1861, May 2021.

[14] M. U. F. Qaisar et al., "Poised: Probabilistic on-demand charging scheduling for ISAC-Assisted WRSNs with multiple mobile charging vehicles," *IEEE Trans. Mobile Comput.*, vol. 23, no. 12, pp. 10818–10834, Dec. 2024.

[15] P. Yang et al., "MORE: Multi-node mobile charging scheduling for deadline constraints," *ACM Trans. Sensor Netw.*, vol. 17, no. 1, pp. 1–21, 2021.

[16] R. Jia, J. Wu, J. Lu, M. Li, F. Lin, and Z. Zheng, "Energy saving in heterogeneous wireless rechargeable sensor networks," in *Proc. IEEE Int. Conf. Comput. Commun.*, 2022, pp. 1838–1847.

[17] Y. Sun et al., "Charging dynamic sensors through online learning," in *Proc. IEEE Int. Conf. Comput. Commun.*, 2023, pp. 1–10.

[18] T. Wu, P. Yang, H. Dai, W. Xu, and M. Xu, "Charging oriented sensor placement and flexible scheduling in rechargeable WSNs," in *Proc. IEEE Int. Conf. Comput. Commun.*, 2019, pp. 73–81.

[19] Y. Liang, H. Wu, and H. Wang, "Asynchronous multi-agent reinforcement learning for collaborative partial charging in wireless rechargeable sensor networks," *IEEE Trans. Mobile Comput.*, vol. 23, no. 5, pp. 4806–4818, May 2024.

[20] T. Liu, B. Wu, S. Zhang, J. Peng, and W. Xu, "An effective multi-node charging scheme for wireless rechargeable sensor networks," in *Proc. IEEE Int. Conf. Comput. Commun.*, 2020, pp. 2026–2035.

[21] W. Huang et al., "Adaptive mobile recharge scheduling with rapid data sharing in wireless rechargeable networks," *IEEE Trans. Mobile Comput.*, vol. 23, no. 4, pp. 3092–3105, Apr. 2024.

[22] J. Zhang et al., "Efficient throughput maximization in dynamic rechargeable networks," *IEEE Trans. Mobile Comput.*, vol. 23, no. 3, pp. 2254–2268, Mar. 2024.

[23] J. Liu et al., "Maximizing sensor lifetime via multi-node partial-charging on sensors," *IEEE Trans. Mobile Comput.*, vol. 22, no. 11, pp. 6571–6584, Nov. 2023.

[24] X. Wang et al., "Practical heterogeneous wireless charger placement with obstacles," *IEEE Trans. Mobile Comput.*, vol. 19, no. 8, pp. 1910–1927, Aug. 2020.

[25] W. You et al., "Practical charger placement scheme for wireless rechargeable sensor networks with obstacles," *ACM Trans. Sensor Netw.*, vol. 20, no. 1, pp. 1–23, 2024.

[26] C. Lin, F. Gao, H. Dai, J. Ren, L. Wang, and G. Wu, "Maximizing charging utility with obstacles through fresnel diffraction model," in *Proc. IEEE Int. Conf. Comput. Commun.*, 2020, pp. 2046–2055.

[27] W. Yang et al., "Precise wireless charging in complicated environments," *IEEE/ACM Trans. Netw.*, vol. 32, no. 6, pp. 4944–4959, Dec. 2024.

[28] Powercast. [Online]. Available: https://www.powercastco.com/

[29] D. Vasisht, S. Kumar, and D. Katabi, "Decimeter-level localization with a single WiFi access point," in *PRoc. USENIX Symp. Netw. Syst. Des. Implementation*, 2016, pp. 165–178.

[30] C. Feng et al., "WiMi: Target material identification with commodity Wi-Fi devices," in *Proc. IEEE Int. Conf. Distrib. Comput. Syst.*, 2019, pp. 700–710.

[31] Z. Luo, Q. Zhang, Y. Ma, M. Singh, and F. Adib, "3D backscatter localization for fine-grained robotics," in *Proc. USENIX Symp. Netw. Syst. Des. Implementation*, 2019, pp. 765–782.

[32] J. Wang, J. Xiong, X. Chen, H. Jiang, R. K. Balan, and D. Fang, "Simultaneous material identification and target imaging with commodity RFID devices," *IEEE Trans. Mobile Comput.*, vol. 20, no. 2, pp. 739–753, Feb. 2021.

[33] S. He, J. Chen, F. Jiang, D. K. Yau, G. Xing, and Y. Sun, "Energy provisioning in wireless rechargeable sensor networks," *IEEE Trans. Mobile Comput.*, vol. 12, no. 10, pp. 1931–1942, Oct. 2013.

[34] T. Koppel, A. Shishkin, H. Haldre, N. Toropovs, I. Vilcane, and P. Tint, "Reflection and transmission properties of common construction materials at 2.4 GHz frequency," *Energy Procedia*, vol. 113, pp. 158–165, 2017.

[35] Z. Zhang, K. Mu, L. Zhang, and C. Zhang, "Measuring the phase shift and polarity reversal of terahertz pulse due to half-wave loss," in *Proc. SPIE Int. Symp. Photoelectronic Detection Imag.*, 2011, pp. 466–471.

[36] D. K. Cheng et al., *Field and Wave Electromagnetics*. Noida, Uttar Pradesh, India: Pearson Education, 1989.

[37] T. Liu et al., "Concurrent charging with wave interference for multiple chargers," *IEEE/ACM Trans. Netw.*, vol. 32, no. 3, pp. 2525–2538, Jun. 2024.

[38] K. M. Donnell and R. Zoughi, "Application of embedded dual-loaded modulated scatterer technique (MST) to multilayer structures," *IEEE Trans. Instrum. Meas.*, vol. 61, no. 10, pp. 2799–2806, Oct. 2012.

[39] D. J. Rosenkrantz, R. E. Stearns, and P. M. Lewis II, "An analysis of several heuristics for the traveling salesman problem," *SIAM J. Comput.*, vol. 6, no. 3, pp. 563–581, 1977.

[40] H. Zhang and Y. Vorobeychik, "Submodular optimization with routing constraints," in *Proc. AAAI Conf. Artif. Intell.*, 2016, pp. 819–825.

[41] A. Ishimaru, *Electromagnetic Wave Propagation, Radiation, and Scattering: From Fundamentals to Applications*. Hoboken, NJ, USA: John Wiley & Sons, 2017.

[42] C. Lin, Z. Yang, H. Dai, L. Cui, L. Wang, and G. Wu, "Minimizing charging delay for directional charging," *IEEE/ACM Trans. Netw.*, vol. 29, no. 6, pp. 2478–2493, Dec. 2021.

[43] S. Wu, H. Dai, L. Liu, L. Xu, F. Xiao, and J. Xu, "Cooperative scheduling for directional wireless charging with spatial occupation," *IEEE Trans. Mobile Comput.*, vol. 23, no. 1, pp. 286–301, Jan. 2024.

[44] C. Lin et al., "Near optimal charging schedule for 3-D wireless rechargeable sensor networks," *IEEE Trans. Mobile Comput.*, vol. 22, no. 6, pp. 3525–3540, Jun. 2023.

[45] Y. Sun et al., "Recycling wasted energy for mobile charging," in *Proc. IEEE 29th Int. Conf. Netw. Protoc.*, 2021, pp. 1–11.

[46] C. Lin et al., "Maximizing charging efficiency with fresnel zones," *IEEE Trans. Mobile Comput.*, vol. 23, no. 1, pp. 612–629, Jan. 2024.

[47] C. Lin et al., "Maximizing charging utility with fresnel diffraction model," *IEEE Trans. Mobile Comput.*, vol. 23, no. 12, pp. 11685–11699, Dec. 2024.

Jing Gao received the BS degree in energy chemical engineering from the Beijing Institute of Technology, Beijing, China, in 2020. She is currently working toward the MS degree with the College of Computer Science, Sichuan Normal University. Her research interest is wireless charging.

Die Wu (Member, IEEE) received the BS degree in information security and the PhD degree in computer architecture from the Electronic Science and Technology of China, in 2011 and 2018, respectively. From 2016 to 2017, he was with the Nanyang Technological University, Singapore, as a visiting PhD Student. He is currently an assistant professor with the College of Computer Science, Sichuan Normal University, Chengdu, China. His research interests include RFID systems, wireless networks, and pervasive computing.

Linglin Zhang received the BS degree in software engineering from Sichuan Normal University, China, in 2023. She is currently working toward the master's degree in software engineering in Sichuan Normal University. Her research interests include wireless charging and wireless sensor networks.

Jingwen Li received the bachelor's degree in computer science from the University of Electronic Science and Technology of China, China, in 2018, and the PhD degree from the Department of Industrial Systems Engineering and Management, National University of Singapore, in 2022 She is currently a lecturer with the Department of Computer Science, Sichuan Normal University. Her research focuses on deep reinforcement learning for combinatorial optimization problems, especially for vehicle routing problems.

Jin Yang received the MS and PhD degrees in computer science from Sichuan University, Sichuan, China, in 2004 and 2007 respectively. He is currently an associate professor with the School of Cyber Science and Engineering, Sichuan University, China. His main research interests include network security, knowledge discovery, and artificial intelligence.

Jian Peng (Member, IEEE) received the BA and PhD degrees from the University of Electronic Science and Technology of China (UESTC) in 1992 and 2004, respectively. He is a professor with the College of Computer Science, Sichuan University. His recent research interests include wireless sensor networks, Big Data, and cloud computing.

Tang Liu (Member, IEEE) received the BS degree in computer science from the University of Electronic and Science of China, China, in 2003, and the MS and PhD degree in computer science from Sichuan University in 2009 and 2015, respectively. Since 2003, he has been with the College of Computer Science, Sichuan Normal University, where he is currently a professor. He has authored more than 50 scientific papers in several journals and conferences, including IEEE INFOCOM, *IEEE Transactions on Mobile Computing*, *IEEE/ACM Transactions on Networking*, *IEEE Transactions on Wireless Communications*, *ACM Transactions on Sensor Networks*, *IEEE Transactions on Communications* and IEEE IPDPS. His research interests include wireless charging, Internet of Things, and wireless sensor networks.